Organic & Biomolecular Chemistry

Cite this: *Org. Biomol. Chem.*, 2012, **10**, 3924

www.rsc.org/obc

PAPER

Hydroxylation mechanism of methane and its derivatives over designed methane monooxygenase model with peroxo dizinc core†

Cai-Qin Li,[a] Hua-Qing Yang,*[a] Jian Xu[a] and Chang-Wei Hu[b]

Received 20th January 2012, Accepted 13th March 2012
DOI: 10.1039/c2ob25163a

The peroxo dizinc Zn_2O_2 complex Q coordinated by imidazole and carboxylate groups for each Zn center has been designed to model the hydroxylase component of methane monooxygenase (MMO) enzyme, on the basis of the experimentally available structure information of enzyme with divalent zinc ion and the MMO with Fe_2O_2 core. The reaction mechanism for the hydroxylation of methane and its derivatives catalyzed by Q has been investigated at the B3LYP*/cc-pVTZ, Lanl2tz level in protein solution environment. These hydroxylation reactions proceed *via* a radical-rebound mechanism, with the rate-determining step of the C–H bond cleavage. This radical-rebound reaction mechanism is analogous to the experimentally available MMOs with diamond Fe_2O_2 core accompanied by a coordinate number of six for the hydroxylation of methane. The rate constants for the hydroxylation of substrates catalyzed by Q increase along $CH_4 < CH_3F < CH_3CN \approx CH_3NO_2 < CH_3CH_3$. Both the activation strain $\Delta E^{\neq}_{strain}$ and the stabilizing interaction $\Delta E^{\neq}_{int}$ jointly affect the activation energy $\Delta E^{\neq}$. For the C–H cleavage of substrate CH_3X, with the decrease of steric shielding for the substituted CH_3X (X = F > H > CH_3 > NO_2 > CN) attacking the O center in Q, the activation strain $\Delta E^{\neq}_{strain}$ decreases, whereas the stabilizing interaction $\Delta E^{\neq}_{int}$ increases. It is predicted that the MMO with peroxo dizinc Zn_2O_2 core should be a promising catalyst for the hydroxylation of methane and its derivatives.

I. Introduction

Under ambient temperature and moderate pressure, the hydroxylase component (MMOH) of the methane monooxygenase (MMO) enzyme can catalyze the hydroxylation of the C–H bond in a wide range of substrates, including methane.[1,2] The reactivity of the enzyme can be tuned by using different metal ions with specific redox states, different ligands or geometric arrangements, and a particular protein environment.[3–5] In recent years, there has been an increasing interest in the redesign of existing metal-binding sites in proteins and the introduction of metals into folded proteins/peptides. In particular, the new design of artificial metalloproteins has contributed significantly to our understanding of the fundamental principles of chemistry and biology governing protein folding, while simultaneously laying the groundwork for the development of novel catalysts and biosensors.

Naturally, MMO exists in some methanotrophic bacteria as an iron-containing soluble form (sMMO) and a copper-containing particulate form (pMMO).[6,7] A number of synthetic MMOs can be competent to selectively catalyze the hydroxylation of hydrocarbons with the same transition metal (iron or copper) which is bound to the same protein and amino acid molecules as the natural MMO.[8,9] Moreover, in the chemical system the metal-binding sites can be also chosen among potential metals, *e.g.* dicobalt,[3,4] dimanganese,[3,4,10] and diruthenium[5] forms of MMO. Although a zinc-containing MMO has not yet been reported experimentally, a zinc-based catalyst seems to be more promising because it is capable of transferring the activated oxygen to the ligated hydrocarbon by zinc centre.[11,12]

Extensive experimental and theoretical studies of MMO have been recently carried out, thereby contributing substantially toward the elucidation of various steps in the catalytic cycle at an atomic level in detail. The key intermediate Q, which is generated in the MMOH catalytic cycle, is competent to hydroxylate methane, various substituted methane, and other hydrocarbons. Generally, the proposed reaction mechanisms of intermediate Q containing the $Fe_2(\mu\text{-}O)_2$ core with methane involves three different classes: radical-rebound,[13–17] non-radical,[18,19] and non-synchronous concerted mechanisms.[20] However, the elucidation

[a]*College of Chemical Engineering, Sichuan University, Chengdu, Sichuan610065, P.R. China. E-mail: huaqingyang@scu.edu.cn; Fax: +028-85415608; Tel: +028-85415608*
[b]*Key Laboratory of Green Chemistry and Technology, Ministry of Education, College of Chemistry, Sichuan University, Chengdu, Sichuan610064, P.R. China*

† Electronic supplementary information (ESI) available: Zero-point energies (*ZPE*) (hartree), total energies (E_e) (hartree) corrected by ZPE, and relative energies (E_r) (kJ mol^{-1}) of various species with respect to reactants at the B3LYP/6-311++G(d, p), Lanl2dz level in protein solution environment. The standard orientations and vibrational frequencies of various species at the B3LYP/6-31G(d, p), Lanl2dz level in the gas phase. See DOI: 10.1039/c2ob25163a

of the actual reaction mechanism of the C–H bond activation in methane catalyzed by sMMO is still an open question and requires further studies, as the concrete reaction mechanism might be affected by using different metal ions.

The present article focuses on designing the model structure of Q with a Zn_2O_2 core, and the reaction mechanism between Q with Zn_2O_2 core and substrates (methane and substituted methane), including the reliable structures and energetics for different reactants, intermediates, transition states (TSs), and products. Furthermore, it is necessary to provide insight into how the designed model Q with the Zn_2O_2 core catalyzes the hydroxylation of different substrates.

II. Computational details

All calculations, including both the structural optimization of the designed model and the hydroxylation mechanism over the modeled Q with Zn_2O_2 core, were performed with the Gaussian 03 programs.[21] Full geometry optimizations were run to locate all of the stationary points and TSs on the singlet spin state potential energy surface (PES) for the reaction of Q + CH_3X (X = H, CH_3, CN, NO_2, and F), using a hybrid B3LYP[22–24] functional method with the 6-31G(d, p)[25,26] basis set for carbon, oxygen, nitrogen, fluorine, and hydrogen, and the Lanl2dz basis set and the corresponding effective core potential (ECP) for zinc, namely B3LYP/6-31G(d, p), Lanl2dz. On the singlet-state PES of Q + CH_3X, the TSs with the single-bond cleavage are reasonably considered to have open-shell singlet electronic configuration. Accordingly, for the TSs, we carried out calculation for open- and closed-shell singlet states using the symmetry-broken spin-unrestricted UB3LYP and spin-restricted RB3LYP methods, respectively, and then compared their energies and chose the species with lower energies to obtain the PES for the lowest singlet state. The stability of the density functional theory (DFT) wavefunction was tested. If an instability is found, the wavefunction is reoptimized with the appropriate reduction in constraints, and the stability tests and reoptimizations are repeated until a stable wavefunction is found.[27,28] Systematic frequency calculations were performed to characterize stationary points obtained and to take corrections of zero-point vibrational energy (ZPE) into account. Each transition state was characterized by the analysis of the normal mode corresponding to its unique imaginary frequency. The natural charge, electron configurations, and dominant occupancies of natural bond orbitals were calculated by the natural bond orbital (NBO) method.[29,30] To estimate the energy effect of protein, solvent effects were taken into account with the 6-311++G(d, p)[31,32] basis set for carbon, oxygen, nitrogen, fluorine, and hydrogen, and the Lanl2dz basis set and the corresponding effective core potential (ECP) for zinc, using B3LYP method, namely B3LYP/6-311++G(d, p), Lanl2dz, by performing single-point calculations on the optimized structures at the B3LYP/6-31G(d, p), Lanl2dz level, using the polarized continuum model (PCM).[33,34] The dielectric constants (ε) were chosen to be 4 (the average effect of both the protein and buried water molecule).[35,36] Finally, the single-point calculations are further performed on the optimized structures at the B3LYP/6-31G(d, p), Lanl2dz level under PCM with ε = 4,[33–36] using B3LYP* functional with 15% exact exchange admixture,[37] with cc-pVTZ basis set for carbon, oxygen, nitrogen, fluorine, and hydrogen,[38] and the Lanl2tz basis set and the corresponding effective core potential (ECP) for zinc.[39] This basis combination is denoted here as B3LYP*/cc-pVTZ, Lanl2tz. Unless otherwise mentioned, all energies are relative to the ground-state reactants (Q + CH_3X) at the B3LYP*/cc-pVTZ, Lanl2tz level including ZPE corrections at the B3LYP/6-311++G(d, p), Lanl2dz level in protein solution environment.

III. Results and discussion

III.1 Structural model Q with Zn_2O_2 core

First, we have to choose a reasonable model for the starting complex, Q. Of the first row transition metals, zinc is very important in enzyme systems. Divalent zinc, Zn^{2+}, is at the borderline between hard and soft cations, and can accommodate nitrogen, oxygen, sulfur, and halogen atoms in its coordination polyhedron. As divalent zinc has a filled d-shell and is not subject to ligand field effects that stabilize octahedral over tetrahedral geometries, zinc ion complexes generally show coordinate numbers of four,[40,41] five,[40,42] and six.[40] According to the experimentally available structure information of enzyme with divalent zinc ion[40–42] and the MMO with bis(μ-oxo) diiron core,[17,18] the working model should satisfy the following conditions: (1) it should include two Zn–Zn bridging oxo ligands, and one histidine acid residue and one didentate terminal carboxylate of glutamic acid residue coordinated ligands for each Zn center; (2) the net charge of the system should be "zero"; and (3) in order to mimic histidine and glutamic acid residues, the ancillary ligands are replaced by imidazole and carboxylate groups, respectively. So, the rather small reasonable model of compound Q satisfying these conditions is *cis*-$(C_3N_2H_4)(COOH)Zn_2O_2(COOH)(C_3N_2H_4)$, which was chosen to be our working model throughout this paper.

The structural optimization of the designed model Q shows that the O(1)–O(2) distance of 1.590 Å is reasonable for a peroxo species, because there is an occupancy of 1.995 *e* in BD(σ)O(1)–O(2) orbital, and the O–O double bond distance is 1.206 Å in the dioxygen molecule. The Zn(1)–Zn(2) distance is 3.352 Å. The four Zn–O bond distances range from 1.9 to 2.1 Å in the Zn_2O_2 core. The present natural atomic charge analysis reasonably indicates that the formal charges of Zn and O atoms in the Zn_2O_2 core should be viewed as +2 and −1, because their NBO charges are calculated to be +1.634 and −0.850, respectively. Then, the complex Q has a μ-η^2:η^2-peroxo form. The geometric structure of model Q with Zn_2O_2 core has been previously reported by us.[43] The geometric structure of Zn_2O_2 core in the peroxo $Zn^{II}Zn^{II}$ complex is similar to that of the Cu_2O_2 core in the peroxo $Cu^{II}Cu^{II}$ complex.[9]

III.2 Reaction mechanism in protein solution

Based on the above designed model Q, we will discuss the following reaction:

$$[Zn_2O_2]_Q + CH_3X \rightarrow [Zn_2(\mu - O)]_P + CH_2XOH \quad (X = H, CH_3, CN, NO_2, \text{and } F)$$

The reaction pathways and the optimized geometries of various species are depicted in Scheme 1. The schematic energy diagrams along the reaction pathways in the hydroxylation of methane, ethane, acetonitrile, nitromethane and fluoromethane are shown in Fig. 1. The Mülliken atomic spin densities are listed in Table 1.

As shown in Fig. 1, the change of Gibbs free energies (ΔG_{298}) of the whole reaction of Q + CH_3X → P + CH_2XOH (X = H, CH_3, CN, NO_2, and F) is calculated to be −177.7, −200.1, −175.1, −204.6, and −244.1 kJ mol^{-1}, respectively. It is indicated that the hydroxylation reactions of all the substrates are thermodynamically preferable by Q with the Zn_2O_2 core. Then,

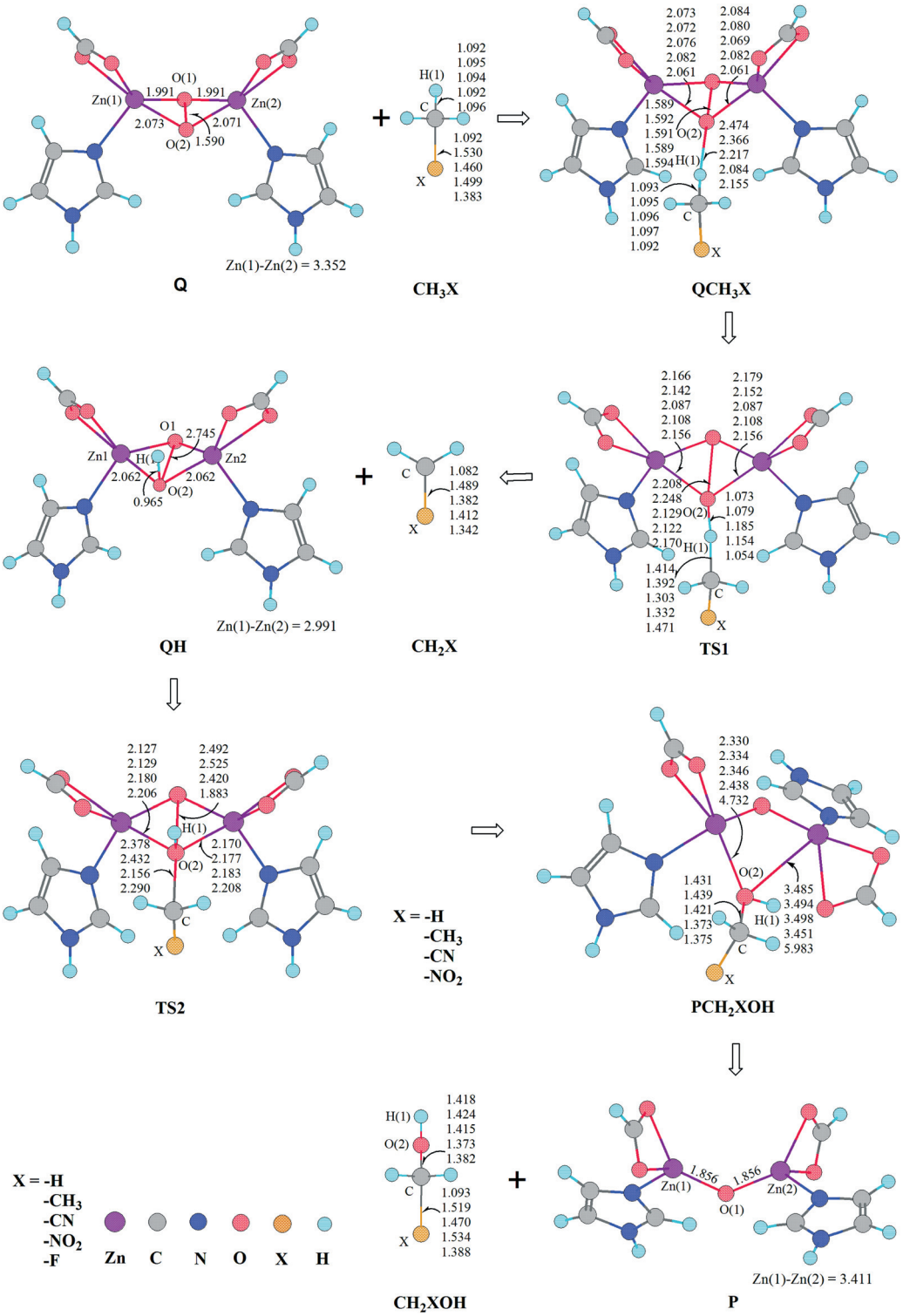

Scheme 1 The reaction pathways and the optimized geometric structures of various species in the hydroxylation reaction of substrates by Q with peroxo dizinc core at the B3LYP/6-31G(d, p), Lanl2dz level in the gas phase. Bond lengths are reported in Å.

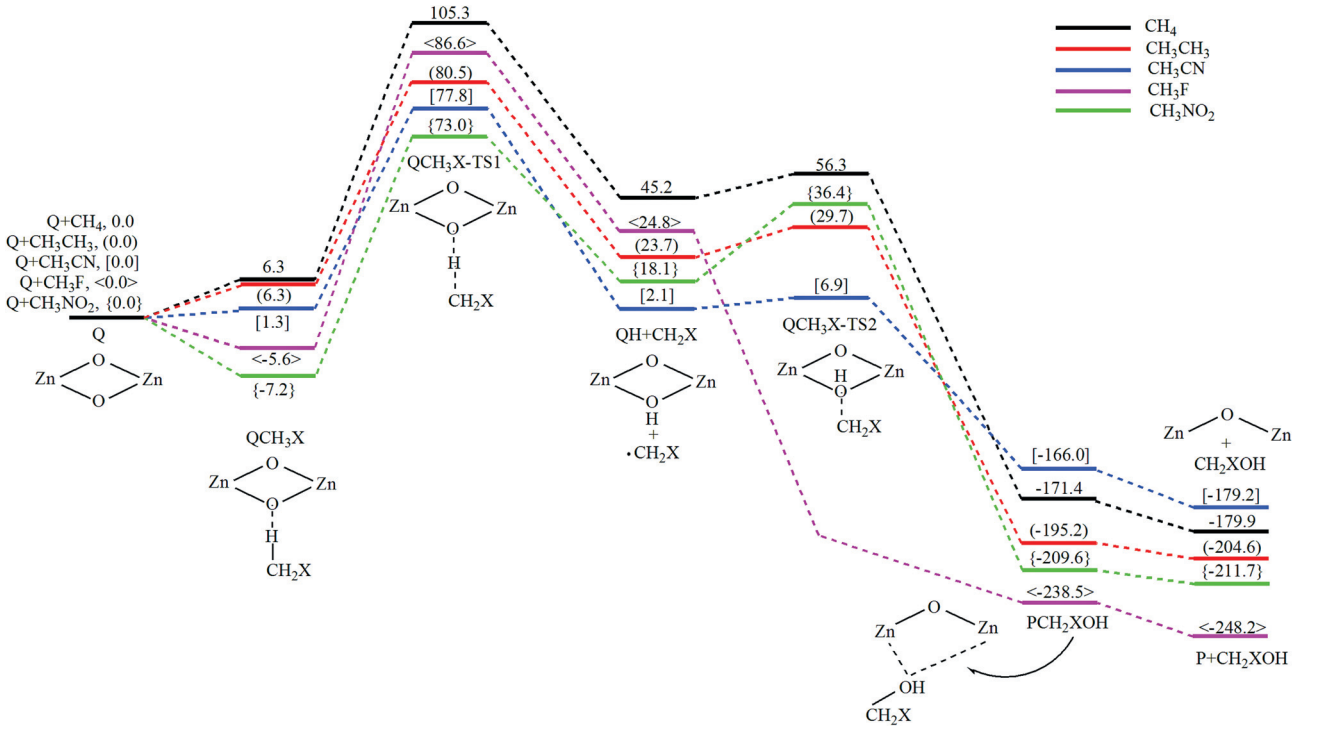

Fig. 1 The schematic energy diagrams along the reaction pathways in the hydroxylation reaction of substrates by Q with peroxo dizinc core at the B3LYP*/cc-pVTZ, Lanl2tz level in the protein solution. Relative energies (kJ mol^{-1}) for the corresponding species relative to Q + CH_3X are shown.

Table 1 Mülliken atomic spin densities of the species in the hydroxylation reaction of substrates by Q with peroxo dizinc core at the B3LYP*/cc-pVTZ, Lanl2tz level in the protein solution environment

Substrate	Species	Zn(1)	Zn(2)	O(1)	O(2)	H(1)	C	X
CH_4	TS1	0.02	0.02	−0.46	0.03	−0.02	0.43	−0.01
	TS2	0.02	0.03	−0.51	−0.20	—	0.69	−0.01
CH_3CH_3	TS1	0.02	0.02	−0.53	0.03	−0.03	0.46	0.03
	TS2	−0.02	−0.03	0.44	0.20	—	−0.58	−0.02
CH_3CN	TS1	0.01	0.01	−0.64	0.27	−0.05	0.34	0.06
	TS2	0.02	0.02	−0.53	−0.10	—	0.47	0.13
CH_3NO_2	TS1	0.01	0.01	−0.65	0.27	−0.05	0.36	0.06
	TS2	0.00	—	−0.29	0.07	—	0.08	0.15
CH_3F	TS1	0.02	0.02	−0.55	0.02	−0.02	0.47	0.04
	QH	−0.01	−0.01	1.00	—	—		

it is necessary to estimate the kinetics for the hydroxylation reaction of the substrates catalyzed by Q with the Zn_2O_2 core.

III.2.1 QCH_3X molecular complex. The hydroxylation of the substrates CH_3X by Q start with the formation of molecular complexes QCH_3X. As shown in Scheme 1, there are two active sites, O(1) and O(2), in model Q. The NBO charges of O(1) and O(2) are calculated to be −0.850. As the O(2)–Zn(1) and O(2)–Zn(2) distances of 2.073 and 2.071 Å are longer than the corresponding O(1)–Zn(1) and O(1)–Zn(2) distances of 1.991 Å in the compound Q, it is reasonable that the O(2) is more active than the O(1) in the formation of the molecular complex QCH_3X. Since the NBO charges of the H atom in CH_3X (X = H, CH_3, CN, NO_2, and F) are calculated to be 0.233, 0.229, 0.280, 0.262, and 0.190, respectively, one can imagine that the H atom with a positive charge in CH_3X approaches the O(2) atom with a negative charge in Q, resulting in the molecular complexes QCH_3X. For CH_3CN and CH_3NO_2, although the NBO charges of the C atom in the –CN group and the N atom in the $–NO_2$ group are calculated to 0.285 and 0.511, respectively, we failed to obtain the corresponding molecular complexes, in which the C atom in the –CN group and the N atom in the $–NO_2$ group approach the O(2) atom with a negative charge in Q. This may be ascribed to the steric shielding of the C atom in the –CN group and the N atom in the $–NO_2$ group attacking the O(2) atom in Q. In QCH_3X (X = H, CH_3, CN, NO_2, and F), the

O(2)–H(1) distance is 2.474, 2.366, 2.217, 2.084, and 2.155 Å, and the corresponding Mülliken overlap population is 0.015, 0.017, 0.026, 0.028, and 0.013, respectively. It is indicated that there is weak interaction between Q and CH_3X in the QCH_3X complex. The complexation energy is calculated to be −6.3, −6.3, −1.3, 7.2, and 5.6 kJ mol^{-1} for QCH_3X (X = H, CH_3, CN, NO_2, and F), respectively. For QCH_4 and QCH_3CH_3, the negative value of complexation energies may be ascribed to poor solubility of non-polar CH_4 and CH_3CH_3 in the polar protein solution. For QCH_3NO_2 and QCH_3F, the O and F atoms with a negative charge easily bind to the positively charged amino acid residues, which makes the molecular complex more stable. This can be testified by the short distances of 2.314 and 2.234 Å in O–H and F–H, and the Mülliken overlap populations of 0.040 and 0.025 for QCH_3NO_2 and QCH_3F, respectively. Nevertheless, for QCH_3NO_2 and QCH_3F, the H-end in CH_3X interaction with the active site O(2) in Q with the Zn_2O_2 core is similar to those for QCH_4, QCH_3CH_3, and QCH_3CN.

III.2.2 C–H bond cleavage. From the molecular complex, QCH_3X, the reaction proceeds through C–H bond cleavage *via* TS1, leading to the QH complex and substituted methyl CH_2X radicals, respectively.

From QCH_3X to TS1, the distinct geometry changes exists in O(1)–O(2), O(2)–H(1), and H(1)–C. Both O(1)–O(2) and H(1)–C distances are evidently elongated, whereas the O(2)–H(1) distance is obviously shortened, as shown in Scheme 1. These results indicate that the interaction of O(2)–H(1) is clearly increased, and the interaction between H(1) and C(1) is evidently weakened. According to NBO analysis at the B3LYP/6-31G(d, p), Lanl2dz level, the charge transfer (CT) at TS1 is 0.451, 0.422, and 0.414 *e* with an ionic character in the Q + CH_3X (X = CH_3, H, and F) reaction systems, respectively, whereas the CT at TS1 is 0.179 and 0.155 *e* with a polar character in the Q + CH_3X (X = CN and NO_2) reaction systems, respectively.[44] In TS1, as shown in Table 1, a radical center begins to develop in the CH_2X (X = H, CH_3, CN, NO_2, and F) group with the spin densities of 0.43, 0.46, 0.34, 0.36, and 0.47 *e* on C(1) atom, and in the QH group with the spin densities of −0.46, −0.53, −0.64, −0.65, and −0.55 *e* on the O(1) atom, respectively. Because all the vibration modes of the unique imaginary frequency of 811i, 603i, 1327i, 1245i, and 949i cm^{-1} correspond to the fact that H(1) gets gradually closer to O(2) and farther away from C(1), the TS1s (X = H, CH_3, CN, NO_2, and F) can be regarded as the late transition states, respectively.

The H-atom abstraction results in the formation of QH complex and substituted methyl CH_2X radicals. In the QH complex, for O(2)–H(1), both the distance (0.965 Å) and the occupancy (1.996 *e*) are characteristics of the formation of an O(2)–H(1) single bond, with the spin density of 1.03 *e* on the O(1) atom. In the substituted methyl CH_2X, the spin densities mainly locate on the C atoms, which clearly demonstrate that the corresponding radicals have been formed.

On the singlet PES, the reaction of Q + CH_3X → QH + CH_2X is calculated to be endothermic by only 45.2, 23.7, 2.1, 18.1, and 24.8 kJ mol^{-1} (X = H, CH_3, CN, NO_2, and F), respectively. It is indicated that these C–H cleavage steps are almost thermodynamically favorable. This reaction step requires an energy barrier of 99.0, 74.2, 76.5, 80.2, and 92.2 kJ mol^{-1} (X = H, CH_3, CN, NO_2, and F), respectively.

III.2.3 Radical-rebound. Next, from QH + CH_2X, the C atom of CH_2X radical rebounds easily to the bridged O(2) atom of QH *via* TS2, leading to the formation of a C–O bond, and then resulting in the molecular complex PCH_2XOH, because there is almost 1.0 *e* spin density on both C and O(1) atoms in the CH_2X and QH moieties. Specially, only TS2s (X = H, CH_3, CN, and NO_2) were obtained, whereas the TS2 (X = F) was not found, despite our extensive attempts.

From QH + CH_2X to TS2, the absolute values of spin density on both O(2) and C atoms are evidently decreased. The C–O(2) distance is obviously shortened to 2.378, 2.432, 2.156, and 2.290 Å (X = H, CH_3, CN, and NO_2), respectively. It is indicated that the C–O(2) covalent bonds were forming. In TS2s (X = H, CH_3, CN, and NO_2), because all the vibration modes of the unique imaginary frequencies of 291i, 223i, 272i, and 304i cm^{-1} correspond to the fact that C gets gradually farther away from O(2) with the QH moiety remaining almost silent, all the TS2s can be regarded as the early transition states, respectively.

The formation of the C–O(2) covalent bond leads to the formation of the PCH_2XOH molecular complex. This can be confirmed by the emergence of almost 2.0 *e* occupancy for the BD(σ)C–O(2) orbital and the approx. 1.4 Å distance of C–O(2) in PCH_2XOH, as shown in Scheme 1.

On the singlet PES, the reaction of QH + CH_2X → PCH_2XOH is calculated to be exothermic by 216.6, 218.9, 168.1, 227.7, and 263.3 kJ mol^{-1} (X = H, CH_3, CN, NO_2, and F), respectively. Such a large exothermicity makes this radical-rebound reaction step thermodynamically preferable. This reaction step involves an energy barrier of 11.1, 6.0, 4.8, and 18.3 kJ mol^{-1} (X = H, CH_3, CN, and NO_2), respectively. Such a low energy barrier makes this reaction step proceed readily.

III.2.4 Release of CH_2XOH from PCH_2XOH. The last step is the release of the CH_2XOH molecule from PCH_2XOH, leaving P behind. In the complex P, the present natural atomic charge analysis reasonably indicates that the formal charges of Zn and O(1) atoms should be viewed as +2 and −2, because their NBO charges are calculated to be +1.573 and −1.551, respectively. Furthermore, both Zn(1)–O(1) and Zn(2)–O(1) distances are 1.856 Å. These results indicate that both the Zn(1)–O(1) and Zn(2)–O(1) ionic bonds have been formed. As depicted in Fig. 1, the corresponding PES is downhill with an exothermicity of 8.5, 9.4, 13.2, 2.1, and 9.7 kJ mol^{-1} (X = H, CH_3, CN, NO_2, and F), respectively, allowing the release of CH_2XOH in a barrierless step.

As shown in Fig. 1, on the singlet PES of the Q + CH_3X → P + CH_2XOH reaction, the energy barrier of the C–H bond cleavage is higher than that of the corresponding radical-rebound step, respectively. Moreover, the energy height of the highest point (EHHP) locates at TS1 on each of the singlet PES. Thereupon, the reaction step of the C–H bond cleavage is the rate-determining step, which involves the activation energy of 105.3, 80.5, 77.8, 73.0, and 86.6 kJ mol^{-1} relative to the dissociation limit (Q + CH_3X) (X = H, CH_3, CN, NO_2, and F), respectively. One can see that the MMO with the peroxo Zn_2O_2 core should be a promising catalyst for the hydroxylation of methane and its

derivatives. Then, it is necessary to provide insight into how substrate properties govern the catalytic hydroxylation reactions catalyzed by Q with Zn_2O_2 core in protein solution (*vide infra*).

III.3 Comparison of the reactivity of different substrates catalyzed by Q

As discussed earlier, C–H bond cleavage is the rate-determining step in the hydroxylation of methane and its derivatives by Q with a peroxo-$Zn^{II}Zn^{II}$ core. To estimate quantitatively the reactivities of different substrates, the rate constants have been evaluated according to conventional transition state theory (TST),[45] including a tunneling correction based on Winger's formulation.[46] Based on the rate-determining step for the hydroxylation of the substrates, the Q + CH_3X were taken as reactants, while the corresponding TS1s severed as transition states, respectively. Over the 280–320 K temperature range, the rate constants of Q + $CH_3X \rightarrow$ P + CH_2XOH can be fitted by the following expressions (1)–(5) (in $dm^3\ mol^{-1}\ s^{-1}$):

$$k_{CH_4} = 4.64 \times 10^4\ \exp(-102\ 030/RT) \quad (1)$$

$$k_{CH_3CH_3} = 3.24 \times 10^6\ \exp(-83\ 621/RT) \quad (2)$$

$$k_{CH_3CN} = 1.96 \times 10^4\ \exp(-76\ 915/RT) \quad (3)$$

$$k_{CH_3NO_2} = 5.22 \times 10^3\ \exp(-72\ 264/RT) \quad (4)$$

$$k_{CH_3F} = 8.60 \times 10^4\ \exp(-86\ 130/RT) \quad (5)$$

The rate constants for the hydroxylation of CH_3CH_3, CH_3NO_2, CH_3CN, and CH_3F are calculated to be 4–5, 3–4, 3–4, and 2–3 orders of magnitude higher than the rate constant for the hydroxylation of CH_4, respectively, over the 280–320 K temperature range. That is to say, the rate constants for the hydroxylation of all the substituted methanes is higher than that of methane. The activation Gibbs free energy in the foregoing expressions (1)–(5) decreases in the order CH_4 (102.0 kJ mol^{-1}) > CH_3F (86.1 kJ mol^{-1}) > CH_3CH_3 (83.6 kJ mol^{-1}) > CH_3CN (76.9 kJ mol^{-1}) > CH_3NO_2 (72.3 kJ mol^{-1}). Alternatively, the pre-exponential factor, which is dependent on the tunneling correction, decreases along CH_3CH_3 > CH_3F > CH_4 > CH_3CN > CH_3NO_2. Both the activation Gibbs free energy and the tunneling correction jointly affect the rate constant. Then, the rate constants for the hydroxylation of CH_3X by Q with the peroxo Zn_2O_2 core increase along $CH_4 < CH_3F < CH_3CN \approx CH_3NO_2 < CH_3CH_3$. Thereby, it is necessary to explore the reactivity intrinsic effect for the hydroxylation of different substrates catalyzed by Q with a peroxo Zn_2O_2 core.

For the different substrates CH_3X catalyzed by Q with a peroxo Zn_2O_2 core, the H-abstraction barrier height values as a function of the strength of the C–H bond that is broken, BDE (C–H), are plotted in Fig. 2. As shown in Fig. 2, the H-abstraction barrier height almost linearly correlates with BDE(C–H). This result is analogous to those in literatures.[47,48] With the increase of BDE(C–H), the H-abstraction barrier height almost increases. However, the H-abstraction barrier height for CH_3NO_2 is slightly lower than that for CH_3CN, while the BDE(C–H) for CH_3NO_2 is higher than that for CH_3CN. This may be due to the stronger stabilizing interaction in TS1 for CH_3NO_2, in comparison with CH_3CN. That is to say, both BDE(C–H) in CH_3X and the stabilizing interaction in TS1 have an effect on the H-abstraction barrier height.

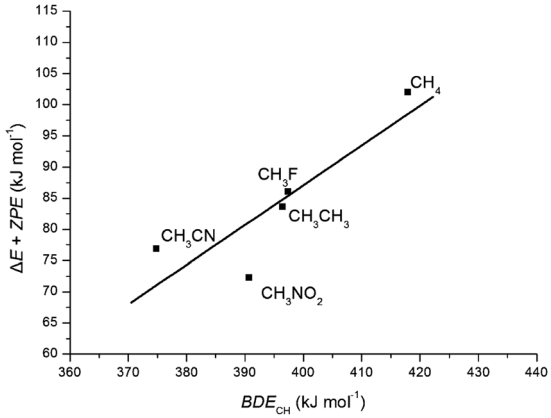

Fig. 2 The H-abstraction barrier heights as a function of the strength of the C–H bond that is broken, BDE(C–H), for different substrates CH_3X catalyzed by Q with a peroxo Zn_2O_2 core.

III.4 Activation strain analysis of C–H bond cleavage

To gain insight into how the substrate affects the activation barriers for the C–H bond cleavage, that is, insight into how this effect depends on the nature of concomitant geometrical deformation and electronic structure of Q and substrate, the trends in reactivity among the C–H cleavage mechanisms are analyzed using the activation strain model of chemical reactivity.[49–51] In this model, activation energies $\Delta E^{\neq}$ of the TS are decomposed into the activation strain $\Delta E^{\neq}_{strain}$ and the stabilizing TS interaction $\Delta E^{\neq}_{int}$: $\Delta E^{\neq} = \Delta E^{\neq}_{strain} + \Delta E^{\neq}_{int}$. The activation strain $\Delta E^{\neq}_{strain}$ is the strain energy associated with deforming the substrate $\Delta E^{\neq}_{strain}$[substr] and the catalyst $\Delta E^{\neq}_{strain}$[cat] from their equilibrium geometry to the geometry they adopt in the TS. The TS interaction $\Delta E^{\neq}_{int}$ is the actual interaction energy between the deformed reactants in the TS.[49–51] Concerning the C–H bond cleavage, the results of the activation strain analysis of TS1s are listed in Table 2.

As shown in Table 2, the activation strain $\Delta E^{\neq}_{strain}$ decreases along CH_3F (205.5 kJ mol^{-1}) > CH_4 (199.6 kJ mol^{-1}) > CH_3CH_3 (159.8 kJ mol^{-1}) > CH_3NO_2 (133.5 kJ mol^{-1}) > CH_3CN (130.2 kJ mol^{-1}). The substrate activation-strain term $\Delta E^{\neq}_{strain}$[substr] also decreases along CH_3F (95.2 kJ mol^{-1}) > CH_4 (78.0 kJ mol^{-1}) > CH_3CH_3 (73.2 kJ mol^{-1}) > CH_3NO_2 (49.8 kJ mol^{-1}) > CH_3CN (43.6 kJ mol^{-1}), which is the same order as the activation strain $\Delta E^{\neq}_{strain}$. It is indicated that the substrate activation-strain term $\Delta E^{\neq}_{strain}$[substr] is characteristic of the activation strain $\Delta E^{\neq}_{strain}$. As depicted in Scheme 1, the typical length of the C–H bond in TS1 decreases along CH_3F (1.471 Å) > CH_4 (1.414) > CH_3CH_3 (1.392) > CH_3NO_2 (1.332) > CH_3CN (1.303 Å). Then, the stretching of the C–H bond in TS1 also decreases along CH_3F (0.375 Å) > CH_4 (0.322) > CH_3CH_3 (0.297) > CH_3NO_2 (0.240) > CH_3CN (0.209 Å). The typical angle of C–H(1)–O(2) in TS1 increases in the order of CH_3F (123.3°) < CH_4 (125.6°) < CH_3CH_3 (138.5°) < CH_3NO_2

Table 2 Geometry (in Å, °) and activation strain analysis of TS1 (in kJ mol^{-1}) for the C–H bond cleavage at the B3LYP/6-311++G(d, p), Lanl2dz level in the protein solution environment

Substrate	C–H(1) length	C–H(1) stretching	C–H(1)–O(2) angle	$\Delta E^{\neq}_{strain}$[substr]	$\Delta E^{\neq}_{strain}$[cat]	$\Delta E^{\neq}_{strain}$	$\Delta E^{\neq}_{int}$	$\Delta E^{\neq}$
CH_4	1.414	0.322	125.6	78.0	121.6	199.6	−94.3	105.3
CH_3CH_3	1.392	0.297	138.5	73.2	86.6	159.8	−79.3	80.5
CH_3CN	1.303	0.209	156.6	43.6	86.6	130.2	−52.4	77.8
CH_3NO_2	1.332	0.240	152.5	49.8	83.7	133.5	−60.5	73.0
CH_3F	1.471	0.375	123.3	95.2	110.3	205.5	−118.9	86.6

(152.5°) < CH_3CN (156.6°). With the C–H(1)–O(2) angle deflation, the activated C–H bond expands, and then the substrate activation-strain term $\Delta E^{\neq}_{strain}$[substr] increases. These geometric characteristics correlate neatly with both the activation strain $\Delta E^{\neq}_{strain}$ and the substrate activation-strain term $\Delta E^{\neq}_{strain}$[substr]. It is indicated that the strain of substrate stems mainly from both C–H bond expansion and C–H(1)–O(2) angle deflation. The reason may be ascribed to more steric shielding for the substituted CH_3X (X = F > H > CH_3 > NO_2 > CN) attacking the O center in Q, resulting in the more concomitant geometrical deformation. In other words, with the decrease of steric shielding for the substituted group of CH_3X attacking the O center in Q, the activation strain $\Delta E^{\neq}$ decreases and then favors the C–H bond cleavage in the order of the substrate CH_3X (X = F < H < CH_3 < NO_2 < CN).

As listed in Table 2, the stabilizing interaction $\Delta E^{\neq}_{int}$ becomes less favorable along the series CH_3F (−118.9 kJ mol^{-1}) > CH_4 (−94.3 kJ mol^{-1}) > CH_3CH_3 (−79.3 kJ mol^{-1}) > CH_3NO_2 (−60.5 kJ mol^{-1}) > CH_3CN (−52.4 kJ mol^{-1}). That is to say, the stabilizing interaction $\Delta E^{\neq}_{int}$ prefers the C–H cleavage along the series of CH_3X (X = F > H > CH_3 > NO_2 > CN). This result also testifies as the foregoing speculation that the stabilizing interaction in TS1 for CH_3NO_2 is stronger than that for CH_3CN. As mentioned earlier, the activation strain $\Delta E^{\neq}_{strain}$ favors the C–H cleavage along the series of CH_3X (X = F < H < CH_3 < NO_2 < CN). It is indicated that the stabilizing interaction $\Delta E^{\neq}_{int}$ increases with the decrease of activation strain $\Delta E^{\neq}_{strain}$. In other words, both the activation strain $\Delta E^{\neq}_{strain}$ and the stabilizing interaction $\Delta E^{\neq}_{int}$ jointly affect the activation energy $\Delta E^{\neq}$. Then, the activation energy $\Delta E^{\neq}$ decreases along CH_4 (105.3 kJ mol^{-1}) > CH_3F (86.6 kJ mol^{-1}) > CH_3CH_3 (80.5 kJ mol^{-1}) > CH_3CN (77.8 kJ mol^{-1}) > CH_3NO_2 (73.0 kJ mol^{-1}). This activation energy $\Delta E^{\neq}$ is consistent with the activation Gibbs free energy in the foregoing expressions (1)–(5), which decreases in the order CH_4 (102.0 kJ mol^{-1}) > CH_3F (86.1 kJ mol^{-1}) > CH_3CH_3 (83.6 kJ mol^{-1}) > CH_3CN (76.9 kJ mol^{-1}) > CH_3NO_2 (72.3 kJ mol^{-1}). In a word, for the C–H cleavage of substrate CH_3X, with the decrease of steric shielding for the substituted CH_3X (X = F > H > CH_3 > NO_2 > CN) attacking the O center in MMO, the activation strain $\Delta E^{\neq}_{strain}$ decreases, whereas the stabilizing interaction $\Delta E^{\neq}_{int}$ increases.

In summary, the hydroxylation of methane and its derivatives by Q with s peroxo-$Zn^{II}Zn^{II}$ core proceeds *via* a radical-rebound mechanism, in which the C–H bond cleavage is the rate-determining step. This radical-rebound reaction mechanism is analogous to the experimentally available MMOs with a diamond Fe_2O_2 core accompanied by a coordinate number of six for the hydroxylation of methane.[13–17] Alternatively, it is different from the non-radical reaction mechanism, which is involved in the experimentally available MMOs with peroxo Cu_2O_2 and diamond Fe_2O_2 cores with a coordinate number of five for the hydroxylation of methane.[9,18,19] The MMO with the peroxo Zn_2O_2 core should be a promising catalyst for the hydroxylation of methane and its derivatives. Thus, the designed peroxo dizinc Zn_2O_2 complex Q coordinated by imidazole and carboxylate groups for each Zn center is reasonable to model the hydroxylase component of the methane monooxygenase (MMO) enzyme.

IV. Conclusion

The following key points may be made from the results presented here.

(1) On the basis of the experimentally available structure information of enzyme with divalent zinc ion and the MMO with the Fe_2O_2 core, the designed peroxo dizinc Zn_2O_2 complex Q coordinated by imidazole and carboxylate groups for each Zn center is reasonable to model the hydroxylase component of the methane monooxygenase (MMO) enzyme. The MMO with a peroxo Zn_2O_2 core should be a promising catalyst for the hydroxylation of methane and its derivatives.

(2) The hydroxylation of methane and its derivatives by Q with a peroxo Zn_2O_2 core proceeds *via* a radical-rebound mechanism, in which the C–H bond cleavage is the rate-determining step. The rate constants for the hydroxylation of the substrate catalyzed by Q with a peroxo Zn_2O_2 core increase along CH_4 < CH_3F < CH_3CN ≈ CH_3NO_2 < CH_3CH_3.

(3) Both BDE(C–H) in CH_3X and the stabilizing interaction in TS1 have an effect on the H-abstraction barrier height.

(4) Both the activation strain $\Delta E^{\neq}_{strain}$ and the stabilizing interaction $\Delta E^{\neq}_{int}$ jointly affect the activation energy $\Delta E^{\neq}$. For the C–H cleavage of substrate CH_3X, with the decrease of steric shielding for the substituted CH_3X (X = F > H > CH_3 > NO_2 > CN) attacking the O center in MMO, the activation strain $\Delta E^{\neq}_{strain}$ also decreases, whereas the stabilizing interaction $\Delta E^{\neq}_{int}$ increases.

Acknowledgements

The authors are grateful for financial support by the National Natural Science Foundation of China (No. 20503017).

Notes and references

1 M. Merkx, D. A. Kopp, M. H. Sazinsky, J. L. Blazyk, J. Müller and S. J. Lippard, *Angew. Chem., Int. Ed.*, 2001, **40**, 2782–2807.

2 M. H. Baik, M. Newcomb, R. A. Friesner and S. J. Lippard, *Chem. Rev.*, 2003, **103**, 2385–2419.
3 M. H. Sazinsky, M. Merkx, E. Cadieux, S. Tang and S. J. Lippard, *Biochemistry*, 2004, **43**, 16263–16276.
4 S. Geremia, L. D. Costanzo, L. Randaccio, D. E. Engel, A. Lombardi, F. Nastri and W. F. DeGrado, *J. Am. Chem. Soc.*, 2005, **127**, 17266–17276.
5 M. D. Khokhar, R. S. Shukla and R. V. Jasra, *J. Mol. Catal. A: Chem.*, 2009, **299**, 108–116.
6 L. L. Chatwood, J. Müller, J. D. Gross, G. Wagner and S. J. Lippard, *Biochemistry*, 2004, **43**, 11983–11991.
7 R. Balasubramanian and A. C. Rosenzweig, *Acc. Chem. Res.*, 2007, **40**, 573–580.
8 L. G. Beauvais and S. J. Lippard, *Biochem. Biophys. Res. Commun.*, 2005, **338**, 262–266.
9 Y. Shiota and K. Yoshizawa, *Inorg. Chem.*, 2009, **48**, 838–845.
10 J. Xu, H. Q. Yang, S. Qin and C. W. Hu, *J. Theor. Comput. Chem.*, 2010, **9**, 233–247.
11 M. Halmann, A. Frei and A. Steinfeld, *Energy*, 2002, **27**, 1069–1084.
12 Z. S. Su, S. Qin, D. Y. Tang, H. Q. Yang and C. W. Hu, *J. Mol. Struct. (THEOCHEM)*, 2006, **778**, 41–48.
13 H. Basch, K. Mogi, D. G. Musaev and K. Morokuma, *J. Am. Chem. Soc.*, 1999, **121**, 7249–7256.
14 B. D. Dunietz, M. D. Beachy, Y. X. Cao, D. A. Whittington, S. J. Lippard and R. A. Friesner, *J. Am. Chem. Soc.*, 2000, **122**, 2828–2839.
15 P. E. M. Siegbahn, *J. Biol. Inorg. Chem.*, 2001, **6**, 27–45.
16 D. G. Musaev, H. Basch and K. Morokuma, *J. Am. Chem. Soc.*, 2002, **124**, 4135–4148.
17 B. F. Gherman, S. J. Lippard and R. A. Friesner, *J. Am. Chem. Soc.*, 2005, **127**, 1025–1037.
18 K. Yoshizawa and T. Yumura, *Chem.–Eur. J.*, 2003, **9**, 2347–2358.
19 K. Yoshizawa, *Acc. Chem. Res.*, 2006, **39**, 375–382.
20 B. F. Gherman, B. D. Dunietz, D. A. Whittington, S. J. Lippard and R. A. Friesner, *J. Am. Chem. Soc.*, 2001, **123**, 3836–3837.
21 M. J. Frisch, G. W. Trucks, H. B. Schlegel, G. E. Scuseria, M. A. Robb, J. R. Cheeseman, J. A. Montgomery Jr., T. Vreven, K. N. Kudin, J. C. Burant, J. M. Millam, S. S. Iyengar, J. Tomasi, V. Barone, B. Mennucci, M. Cossi, G. Scalmani, N. Rega, G. A. Petersson, H. Nakatsuji, M. Hada, M. Ehara, K. Toyota, R. Fukuda, J. Hasegawa, M. Ishida, T. Nakajima, Y. Honda, O. Kitao, H. Nakai, M. Klene, X. Li, J. E. Knox, H. P. Hratchian, J. B. Cross, C. Adamo, J. Jaramillo, R. Gomperts, R. E. Stratmann, O. Yazyev, A. J. Austin, R. Cammi, C. Pomelli, J. W. Ochterski, P. Y. Ayala, K. Morokuma, G. A. Voth, P. Salvador, J. J. Dannenberg, V. G. Zakrzewski, S. Dapprich, A. D. Daniels, M. C. Strain, O. Farkas, D. K. Malick, A. D. Rabuck, K. Raghavachari, J. B. Foresman, J. V. Ortiz, Q. Cui, A. G. Baboul, S. Clifford, J. Cioslowski, B. B. Stefanov, G. Liu, A. Liashenko, P. Piskorz, I. Komaromi, R. L. Martin, D. J. Fox, T. Keith, M. A. Al-Laham, C. Y. Peng, A. Nanayakkara, M. Challacombe, P. M. W. Gill, B. Johnson, W. Chen, M. W. Wong, C. Gonzalez and J. A. Pople, *GAUSSIAN 03 (Revision B.05)*, Gaussian, Inc., Pittsburgh PA. 2003.
22 A. D. Becke, *Phys. Rev. A*, 1988, **38**, 3098–3100.
23 C. Lee, W. T. Yang and R. G. Parr, *Phys. Rev. B: Condens. Matter*, 1988, **37**, 785–789.
24 B. Miehlich, A. Savin, H. Stoll and H. Preuss, *Chem. Phys. Lett.*, 1989, **157**, 200–206.
25 G. A. Petersson and M. A. Al-Laham, *J. Chem. Phys.*, 1991, **94**, 6081–6090.
26 G. A. Petersson, A. Bennett, T. G. Tensfeldt, M. A. Al-Laham, W. A. Shirley and J. Mantzaris, *J. Chem. Phys.*, 1988, **89**, 2193–2218.
27 R. Seeger and J. A. Pople, *J. Chem. Phys.*, 1977, **66**, 3045–3050.
28 R. Bauerschmitt and R. Ahlrichs, *J. Chem. Phys.*, 1996, **104**, 9047–9052.
29 A. E. Reed, L. A. Curtiss and F. Weinhold, *Chem. Rev.*, 1988, **88**, 899–926.
30 A. E. Reed, R. B. Weinstock and F. Weinhold, *J. Chem. Phys.*, 1985, **83**, 735–746.
31 R. Krishnan, J. S. Binkley, R. Seeger and J. A. Pople, *J. Chem. Phys.*, 1980, **72**, 650–654.
32 A. D. Mclean and G. S. Chandler, *J. Chem. Phys.*, 1980, **72**, 5639–5648.
33 E. Cancès, B. Mennucci and J. Tomasi, *J. Chem. Phys.*, 1997, **107**, 3032–3041.
34 M. Cossi, G. Scalmani, N. Rega and V. Barone, *J. Chem. Phys.*, 2002, **117**, 43–54.
35 W. G. Han and L. Noodleman, *Inorg. Chem.*, 2008, **47**, 2975–2986.
36 P. E. M. Siegbahn, *Inorg. Chem.*, 1999, **38**, 2880–2889.
37 M. Reiher, O. Salomon and B. A. Hess, *Theor. Chem. Acc.*, 2001, **107**, 48–55.
38 W. A. de Jong, R. J. Harrison and D. A. Dixon, *J. Chem. Phys.*, 2001, **114**, 48–53.
39 L. E. Roy, P. J. Hay and R. L. Martin, *J. Chem. Theory Comput.*, 2008, **4**, 1029–1031.
40 C. W. Bock, A. K. Katz and J. P. Glusker, *J. Am. Chem. Soc.*, 1995, **117**, 3754–3765.
41 J. Zhou, P. Tao, J. F. Fisher, Q. Shi, S. Mobashery and H. B. Schlegel, *J. Chem. Theory Comput.*, 2010, **6**, 3580–3587.
42 J. Koca, C. G. Zhan, R. C. Rittenhouse and R. L. Ornstein, *J. Comput. Chem.*, 2003, **24**, 368–378.
43 J. Xu, C. Gao, H.-Q. Yang, S. Qin and C. W. Hu, *Chem. Res. & Appl. (in Chinese)*, 2009, **21**, 877–882.
44 L. R. Domingo and J. A. Sáez, *Org. Biomol. Chem.*, 2009, **7**, 3576–3583.
45 H. Eyring, *J. Chem. Phys.*, 1935, **3**, 107–115.
46 E. Wigner, *J. Chem. Phys.*, 1937, **5**, 720–725.
47 J. M. Mayer, *Acc. Chem. Res.*, 1998, **31**, 441–450.
48 S. P. de Visser, *J. Am. Chem. Soc.*, 2010, **132**, 1087–1097.
49 F. M. Bickelhaupt, *J. Comput. Chem.*, 1999, **20**, 114–128.
50 W. J. van Zeist, R. Visser and F. M. Bickelhaupt, *Chem.–Eur. J.*, 2009, **15**, 6112–6115.
51 W. J. van Zeist and F. M. Bickelhaupt, *Org. Biomol. Chem.*, 2010, **8**, 3118–3127.